

# Multi-Source Third Generation Computed Tomography for Industrial Multiphase Flows Applications

Carlos Henrique de Mesquita, Pablo A. Salvador Vasquez, Wilson A.P. Calvo, Larissa A. Marcato, Diego V.S. Carvalho, João F. T. Martins and Margarida M. Hamada.

**Abstract** – This work describes a multi-source computed tomography. It showed to be a feasible tool to study multiphase systems. In this CT scanner, two different radioactive sources,  $^{192}\text{Ir}$  and  $^{137}\text{Cs}$ , were placed together into a single lead collimated system. The CT is capable to determine and differentiate the attenuation coefficients of materials constituted of three phases (gas, liquid and solid), using two or more different radioisotope energies.

## I - INTRODUCTION

Nowadays, a wide range of chemical and petrochemical industries is of great interest to be used in the industrial computed tomography for improving design, operation, optimization and troubleshooting of industrial processes [1,2]. Some physico-chemical processes and industrial products, such as the distillation columns and the combustion engines, involve processes in which materials are found in mixtures of liquids, gases and solids in fast dynamics (Fig. 1).

### The tomography used in industry and their choice.

Despite the great success of the CT in medicine, its use in the industrial application is still in its infancy. The cause is due to the complexity and multiplicity of industrial objects when compared with the human body which is relatively standard.

Currently, there are basically four versions of scanners for industrial purposes, which the third-generation CT scanner and the fourth are the most important and used. Briefly, the third generation CT scanner has better performance in spatial resolution while the fourth-generation CT scanner has the best performance in the temporal resolution, in other words it is capable to generate images more quickly but with poor spatial resolution. If the spatial resolution is important and the knowledge of the dynamic phenomena can be limited to their trends thus the third generation CT may be the better choice.

This work will introduce an improvement in the detection system of industrial CT scanners of the third generation type. Firstly, the principle of the third generation

tomography will be explained. Fig. 2 summarizes the third generation tomography principle.

### Problems and Solutions

The distillation columns and the engines are usually built with steel and have large diameters or thicknesses that make their analysis with conventional X-ray beam unfeasible. For this reason, gamma sources, in the energy range from  $\sim 300$  keV to  $\sim 1500$  keV are preferable to the X-ray beams. By definition, a multiphase system tomography involves objects containing materials with a large array of different densities (solid, liquid and gas mixtures). The low-energy radiation is more sensitive to work in low-density materials, such as gases. Radiation with intermediate energy will be more efficient to evaluate materials such as water, oils and other liquids with a density close to  $\sim 1$  g/cm<sup>3</sup>, while high-energy radiation is more appropriate to evaluate high-density materials. Fig. 3 summarizes these statements.

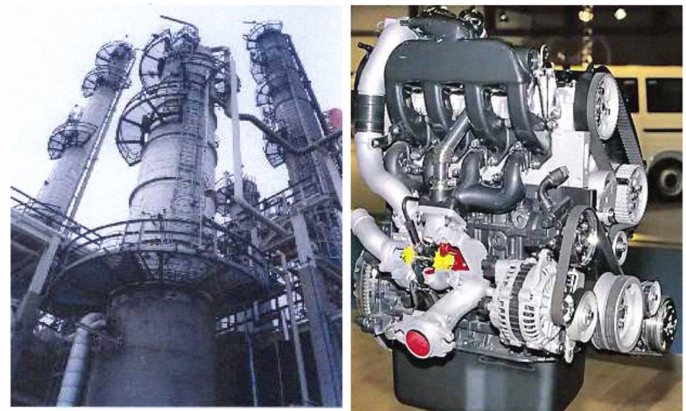


Fig. 1 - Petrochemical distillation columns and combustion engines are examples of multiphase systems. Both contain fractions of liquids (water and oils), gases, and solids in dynamic processes.

The  $\mu$  parameter in the exponential attenuation law depends on the material density. Generically, material with high-density implies a reduction of the transmitted beam. On another point of view, high energy photons produce higher emergent gamma flow. As a result, for objects containing different density materials, ideally, the tomographic measurement should be carried out with different energy gamma rays. In this case, it is recommended that the CT data acquisition system may have the ability to discriminate different energy levels. Commonly, the arrangement with  $^{192}\text{Ir}$  ( $\sim 317$  keV) and  $^{192}\text{Ir}$  (468 keV),  $^{137}\text{Cs}$  (662 keV) and  $^{60}\text{Co}$  (1173 and 1332 keV) sources meets this need. Alternatively, one unique radioisotope source can be used,

Manuscript received November 22, 2011. This work was supported in part by the FAPESP, CNPq and IAEA.

Carlos Henrique de Mesquita and Margarida Mizue Hamada are with the IPEN/CNEN-SP, Av. Prof. Lineu Prestes, 2242 - Cidade Universitária, 05508-000, São Paulo, Brazil. (Tel: + 55-11-3133-9806; e-mail: chmesqui@usp.br).

since it has suitable spectral profile and well distributed energetic multi-peaks, like  $^{75}\text{Se}$ .

Some laboratories use two radioactive sources, with two sets of counters and detectors (Fig. 4(a)), lagged by 90 degrees [6]. This option has the inconvenience of needing double amount of detectors and of single-channel counters. Alternatively, fast multichannel counters can be used, allowing reducing the number of shielded sources, detectors

and counters to be used. This last option meets the needs of the CT for multiphase efficiently. In this work, it is described the use of two different radioactive sealed sources,  $\sim 500$  mCi of  $^{192}\text{Ir}$  ( $\sim 317$  keV and 468 keV) and  $\sim 70$  mCi of  $^{137}\text{Cs}$  (662 keV) placed together into a single lead shielding. For this project we developed an economical and fast data acquisition system based on multichannel analyzers.

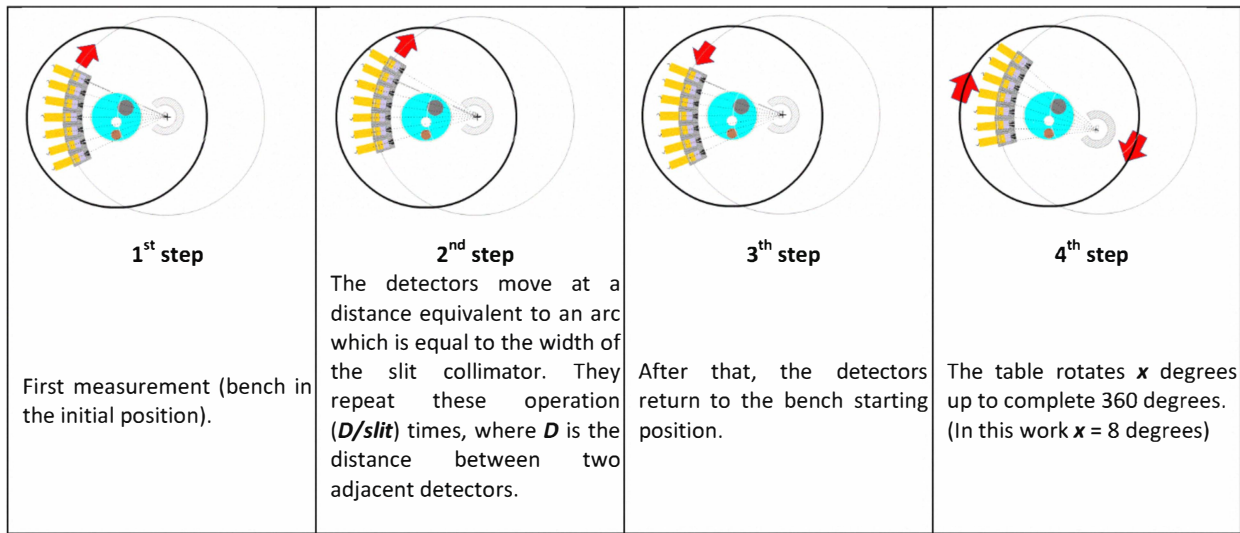


Fig. 2 - Basic principle of operation of the third generation tomography.

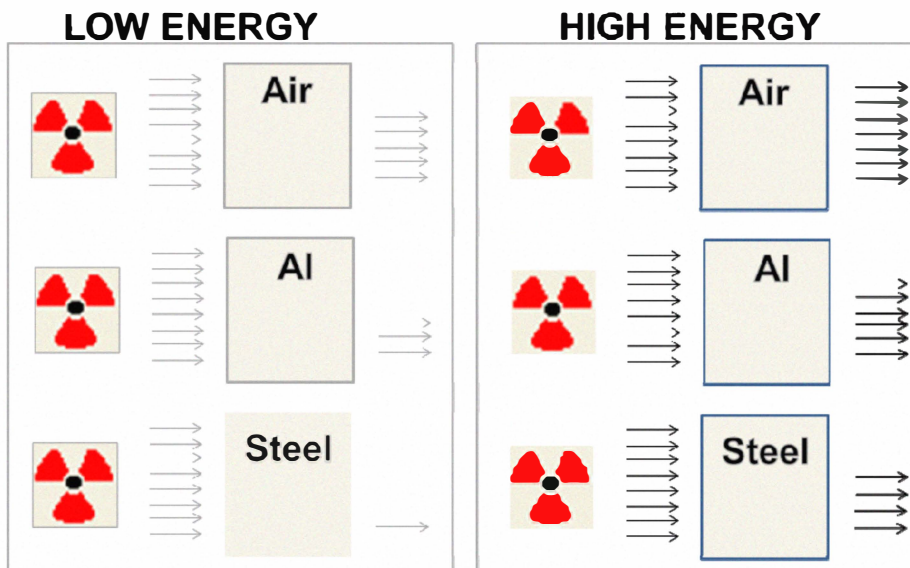
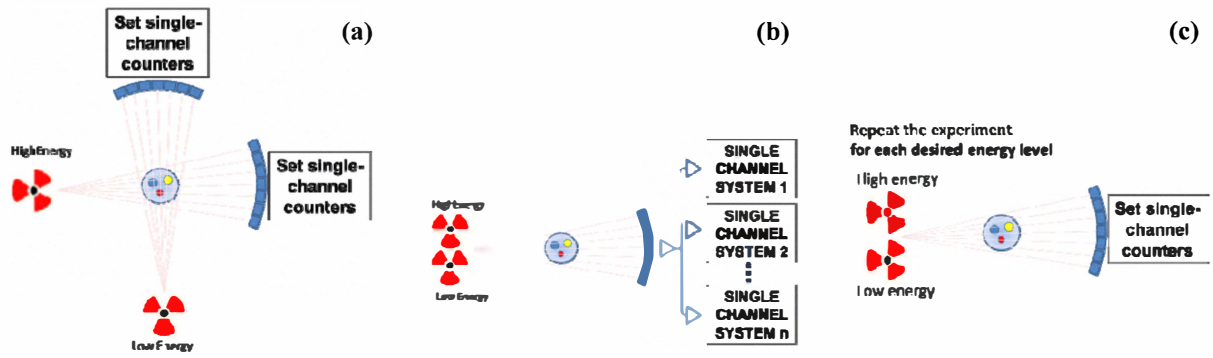


Fig. 3 - A narrow beam of monoenergetic photons with an incident intensity  $I_0$ , penetrating a layer of material with mass thickness  $x$  and density  $\rho$ , emerges with intensity  $I$  given by the exponential attenuation law  $I = I_0 \cdot e^{-\left(\frac{\mu}{\rho}x\right)}$ .



- Need double detectors ( $\uparrow$  cost).
- Need double counters ( $\uparrow$  cost).
- Need double shielded source ( $\uparrow$  cost).
- Need a lot of counters ( $\uparrow$  cost).
- It is limited to each spectral region. For each region of energy is necessary to add another set of counters ( $\uparrow$  cost).
- Low cost, but requires very long measurement time.

Fig. 4 - Some techniques to produce tomographic measurements at different gamma energy regions.

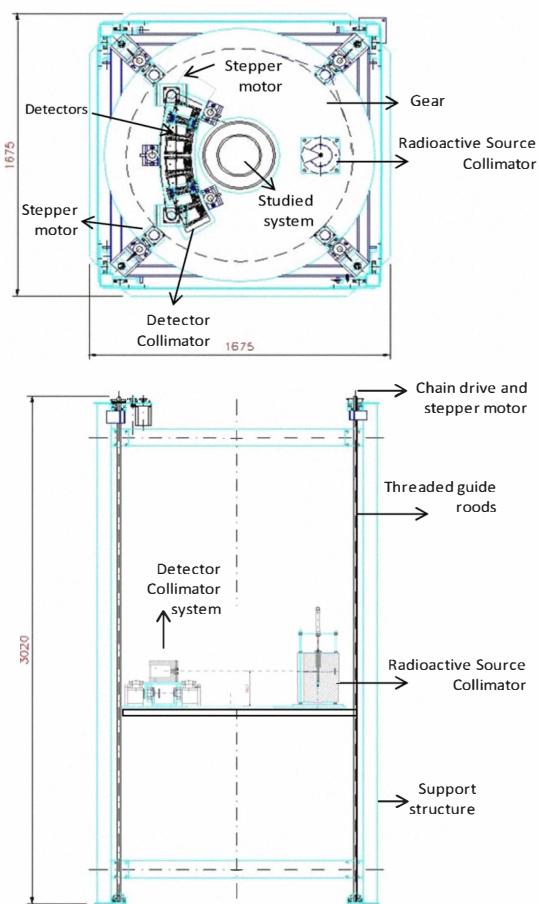


Fig. 5 - Tomographic system. Schematic (left) and actual (right).

## II - MATERIAL AND METHODS

A tomographic scanner, classified as third-generation type, where the collimated detectors are arranged in an arc at the center of the radiation source, was developed in our laboratory [1]. The whole assembly of the detectors and the radiation source are mounted on a gantry capable of being

rotated around the axis of the test section through a stepper motor interfaced with a host computer, as shown in Fig. 5.

The electronic system containing seven multichannel boards (8 bits resolution, 1.5  $\mu$ s time resolution), with their individual high voltage (HV) supplies and a circuit to control three step motors, was specially developed for this device (Fig 6). The electronic pulse profile is shown in Fig. 7 and the  $^{192}\text{Ir}$  and  $^{137}\text{Cs}$  spectrometry obtained by the system are shown in Fig. 8.

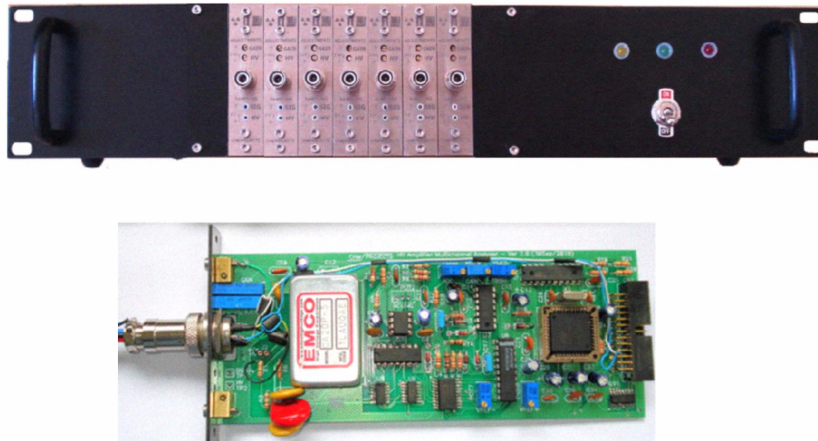


Fig. 6 – The multichannel module (top) and one of seven eight bit resolution multichannel board (bottom).

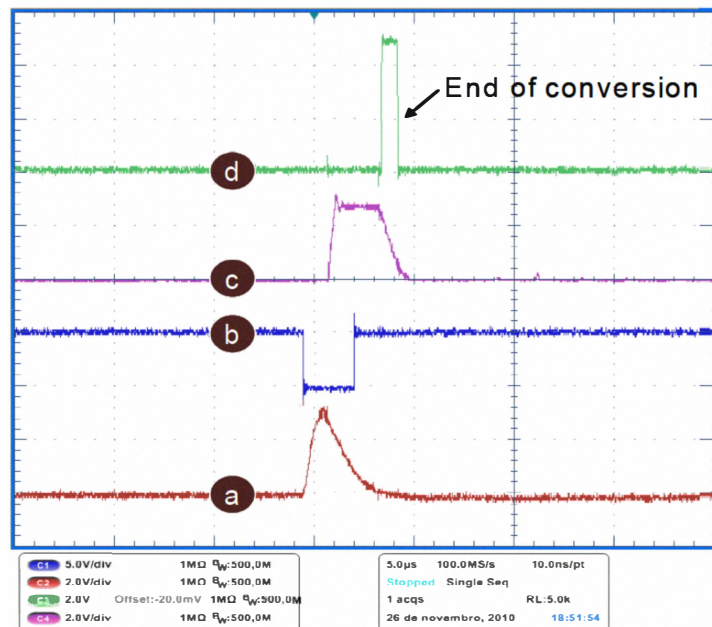


Fig. 7 – Signal profiles MCA (Multichannel analyzer): (a) input signal after last amplification stage, (b) triggering sampling signal, (c) after sample-and hold circuit which is the signal that will be digitized by the ADC and (d) the signal that informs the CPU that the conversion has finished (at the fall edge).

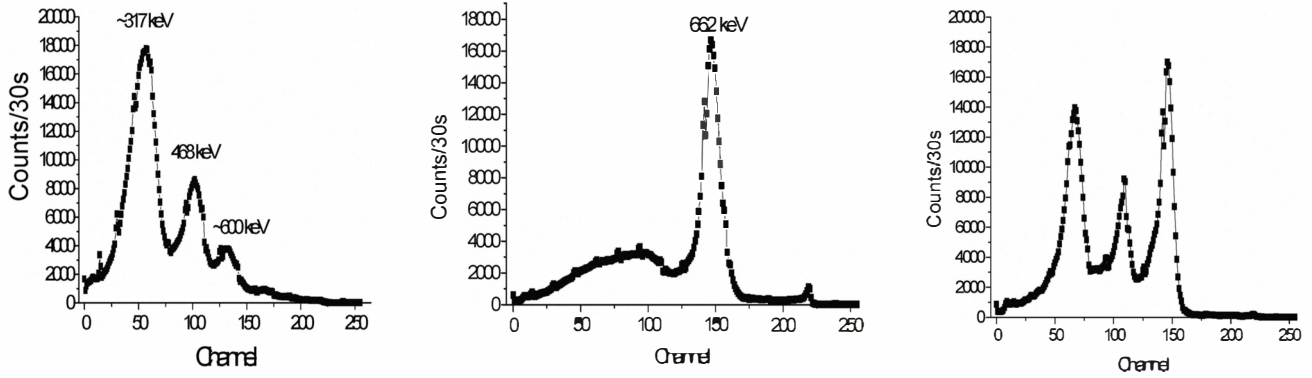


Fig. 8 – Spectrometric profile obtained from the MCA (multichannel) developed:  $^{192}\text{Ir}$  (left),  $^{137}\text{Cs}$  (middle) and  $^{192}\text{Ir}$  plus  $^{137}\text{Cs}$  (right).

The cylindrical lead collimation of the radiation sources provides a narrow fan beam (0.6 cm) with an angle of  $45^\circ$  in the horizontal plane. Seven NaI(Tl) scintillation detectors 2 in. x 2 in. were placed opposite to the radioactive sources (72 cm), always maintaining the fan geometry (Fig. 9). In order to increase the number of projection measurements in one view of the phantom, the number of detectors in the arc was effectively increased by using a collimator that moves across the detector arc.

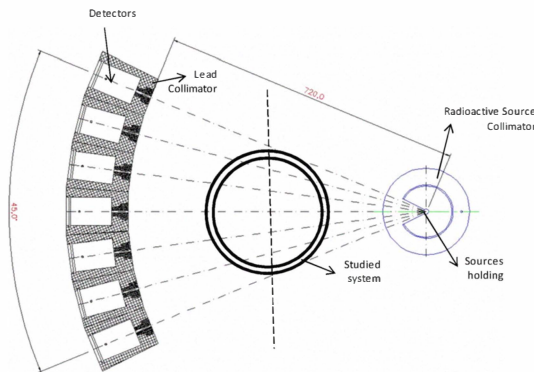


Fig. 9. Configuration of source- detectors

The collimators were made of lead, 5 cm deep and 11.8 cm high, with rectangular holes (slits) of 2x4 mm. These dimensions for the collimator holes were optimized to provide an adequate area for detecting photons with good statistics in the chosen sampling time [2]. The scanner was set for 200 views and 48 projections for each detector (seven), totaling 67,200 projections.

Several algorithms are available for image reconstruction as well as useful software packages that have implemented most of them. In this study, the Alternating Minimization (AM) algorithm proposed for transmission tomography has been applied [3,4]. AM algorithm has been studied extensively in the applications involving X-ray based medical imaging [6]. O’Sullivan and Benac [5] reformulated the Maximum likelihood problem as a double minimization of an I-divergence to obtain a family of image reconstruction algorithms. I-divergence [7], is a measure of

discrepancy between two functions  $f_1(\mathbf{y})$  and  $f_2(\mathbf{y})$  and it is given as:

$$I(f_1||f_2) = \sum_{\mathbf{y} \in \mathcal{Y}} \left[ f_1(\mathbf{y}) \ln \left( \frac{f_1(\mathbf{y})}{f_2(\mathbf{y})} \right) - (f_1(\mathbf{y}) - f_2(\mathbf{y})) \right] \quad (1)$$

where,  $\mathbf{y}$  is a finite dimensional space. This I-divergence measure was first employed for image reconstruction by Snyder et al.[8]: it is relevant for this problem, subject to non-negativity constraints, because the functions involved are all real values, having both positive and negative values that can require to be non-negative. Then, minimizing the least squares is a consistent choice.

Each step of minimization in the AM algorithm is claimed to be an exact process, without any approximation, which represents one of its advantages over other algorithms, as the expectation maximization. The AM algorithm is guaranteed to monotonically increase the log-likelihood function, at every iteration [5]. This image reconstruction algorithm is based on a statistical model for the measured data, Beer’s law and a realistic model for the known point spread function. If  $q(\mathbf{y}; \boldsymbol{\mu})$  is the model for the transmission of gamma photons, following the Beer-Lambert’s law, it is obtained:

$$q(\mathbf{y}; \boldsymbol{\mu}) = I_o(\mathbf{y}) \exp \left( - \sum_{\mathbf{x} \in \mathcal{X}} h(\mathbf{y}|\mathbf{x}) \boldsymbol{\mu}(\mathbf{x}) \right) \quad (2)$$

where,  $I_o(\mathbf{y})$  represents incident photon counts,  $h(\mathbf{y}|\mathbf{x})$  is the point spread function or the length of projection  $\mathbf{y}$  in pixel  $\mathbf{x}$ . In the expression for the I-divergence, the function  $f_1(\mathbf{y})$  is taken to be the measured data represented by a Poisson random number  $d(\mathbf{y})$  and  $f_2(\mathbf{y})$  is taken to be a nonlinear model of  $q(\mathbf{y})$ , representing the transmission of the photons. The term  $q(\mathbf{y}; \boldsymbol{\mu})$  is a function of the attenuation set  $\boldsymbol{\mu}$ , where  $\mathbf{x}$  is the pixel space index. Then, equation (1) can be written as:

$$I(d||q(\mathbf{y}; \boldsymbol{\mu})) = \sum_{\mathbf{y} \in \mathcal{Y}} \left\{ d(\mathbf{y}) \ln \left( \frac{d(\mathbf{y})}{q(\mathbf{y}; \boldsymbol{\mu})} \right) - [d(\mathbf{y}) - q(\mathbf{y}; \boldsymbol{\mu})] \right\} \quad (3)$$

The general objective of the algorithm was stated finding the minimum of  $I(d||q)$  with respect to  $\boldsymbol{\mu}$ :

$$\min_{\mathbf{q} \in \mu} I(\mathbf{d} \parallel \mathbf{q}) \quad (4)$$

The terms in the log-likelihood function that depend on the parameter set (attenuation values to be estimated) are the negative of the corresponding terms in the I-divergence. Thus, minimizing the I-divergence over the parameter set  $\mu$  is equivalent to maximizing the log-likelihood function. Minimizing the I-divergence offers one unique advantage, as it has a known lower bound (equal to zero), for projection data processed from any system. This is not the case when maximizing the log likelihood, since the upper bound is not known.

Minimizing (3) as per (4) yields (5) results in the iterative expression, for updating the parameter set (attenuation values), expressed below:

$$\hat{\mu}^{(k+1)}(x) = \hat{\mu}^{(k)}(x) - \frac{1}{Z(x)} \ln \left( \frac{\tilde{b}(x)}{\hat{b}^{(k)}(x)} \right) \quad (5)$$

The terms with  $\hat{\cdot}$  indicate that it is an estimate of the entity. The terms  $\tilde{b}$  and  $\hat{b}^{(k)}$  are the back projections of  $\mathbf{d}$  and the estimates of  $\hat{q}^{(k)}$ , respectively. On the other hand, they are the back projections of the measured data and the nonlinear model employed (based on Beer-Lamberts law). Their expressions are given by:

$$\tilde{b}(x) = \sum_{y \in Y} h(y|x) d(y) \quad (6)$$

$$\hat{b}^{(k)}(x) = \sum_{y \in Y} h(y|x) \hat{q}^{(k)}(y) \quad (7)$$

where,

$$\hat{q}^{(k)}(y) = I_o(y) \exp \left( - \sum_{x \in X} h(y|x) \hat{\mu}^{(k)}(x) \right) \quad (8)$$

The iterative process for computing the image goes backwards starting from (8) to (5). An initial guess for  $\hat{\mu}^{(k=0)}(x)$  is chosen to calculate  $\hat{q}^{(k)}(y)$  in (8) and then  $\hat{q}^{(k)}(y)$  is used to calculate  $\hat{b}^{(k)}(x)$  in (7). The back projection  $\tilde{b}(x)$  is computed just once, based on the measured data  $\mathbf{d}(y)$ . The term  $\hat{\mu}^{(k+1)}(x)$  is updated based on (5), and the process is started again setting  $k=k+1$  and using the updated values of attenuation. A non-negativity constraint is applied to the values of attenuation. Hence, at any iteration, if  $\hat{\mu}^{(k+1)}(x) < 0$ , it is written as  $\hat{\mu}^{(k+1)}(x) = 0$ .  $Z(x)$  in (5), which is an appropriate scale function chosen for the  $x^{\text{th}}$  pixel, provided the following criterion is satisfied [5]:

$$\sum_{x \in X} \left( \frac{h(y|x)}{Z(x)} \right) \leq 1 \quad (9)$$

For every pixel  $x$ , the length of the longest projection  $y$  passing through it was chosen as the value of  $Z(x)$ , as long as (9) was satisfied. The values of  $Z(x)$  were found to be insensitive to the final convergence values.

The CT capacity to determine and differentiate the attenuation coefficients of materials with three phases (gas, liquid and solid), using two different radioisotope energies, was studied. For this purpose, the AM reconstruction algorithm was carefully selected and used to improve the results.

To validate this CT system, a static phantom built in different materials and containing three phases, gas, liquid and solid, was built (Fig. 10). The phantom was built in acrylic (polymethyl-methacrylate  $(C_5O_2H_8)_n$ , density  $\delta = 1.19 \text{ g/cm}^3$ ) containing an iron cylinder of  $\phi = 20 \text{ mm}$  ( $\delta = 7.87 \text{ g/cm}^3$ ), an aluminum cylinder of  $\phi = 44 \text{ mm}$  ( $\delta = 2.70 \text{ g/cm}^3$ ) and a hollow cylinder of glass ( $\delta = 2.57 \text{ g/cm}^3$ ) with 3.5 mm thick and  $\delta = 50 \text{ mm}$  (Fig. 10).

The results were evaluated related to the theoretical attenuation coefficients and the pixel number values by the root mean squared error (RMSE) in (10).

$$RMSE(\mu) = \sqrt{\frac{\sum_{x \in X} (\hat{\mu}(x) - \mu(x))^2}{\sum \mu(x)^2}} \quad (10)$$

Where  $x$  is the pixel index,  $\hat{\mu}(x)$  are the calculated attenuation values,  $\mu(x)$  are the theoretical attenuation values.

### III RESULTS AND DISCUSSION

The reconstructed CT images yields a map of the attenuation coefficients of the phantom. Fig. 11 (a) shows the results for  $^{192}\text{Ir}$  (317 keV), while Fig. 11 (b) shows the image obtained for  $^{192}\text{Ir}$  (468 keV). The results for  $^{137}\text{Cs}$  (662 keV) is represented in Fig. 11 (c) and finally, the image from data of open window ( $\sim 50 \text{ keV}$  to  $\sim 800 \text{ keV}$ ) is shown in Fig. 11 (d).

According to the classical approach which assumes the  $RMSE(\mu)$  to select the best picture, if in equation (10) is considered the whole object (acrylic, iron, aluminum and air) the  $^{137}\text{Cs}$  shows the best figure of merit = 0.277 (Table 1). However, considering only the image regions containing different materials (iron or aluminum or air) the  $^{192}\text{Ir}$  (317 keV) has better performance for CT analysis in materials like air. Energies in the range of 418 to 662 keV are more suitable for materials with densities closed to aluminum and finally the densest objects such as iron are better evaluated with radiation around 662 keV from  $^{137}\text{Cs}$  (Table 2).

Actually, to study a three-phase ( $n=3$ ) system, two photopeak energies are necessary ( $2=n-1$ ). This is the great advantage of multichannel boards used in this CT, because it is able to work with many radioactive sources placed together in a single shielding. The developed electronic data-acquisition allowed the counting process in different channel regions, simultaneously. Moreover, the multichannel system is fast enough to process signals separated by  $\sim 7.5 \mu\text{s}$  ( $5 \mu\text{s}$  due to electronics (Fig. 7) and  $\leq 2.4 \mu\text{s}$  spent by the microprocessor) and thus can be measured count rates of up to 133,000 counts per second. This performance qualifies this multichannel system to operate in the industrial gamma tomography.

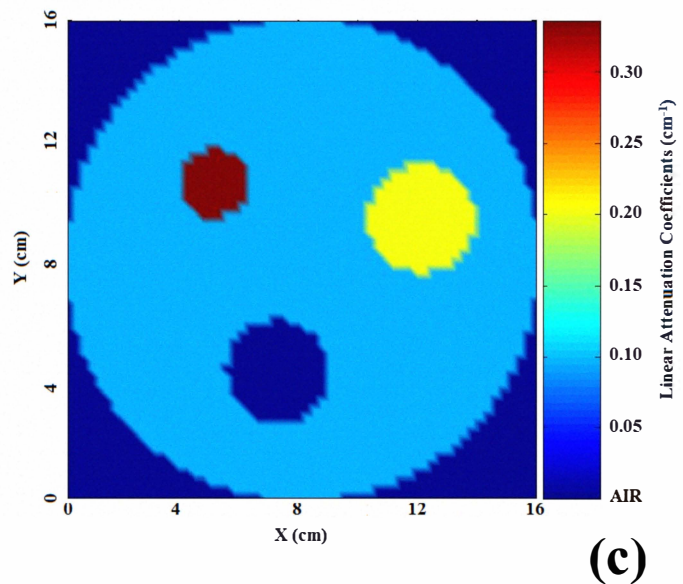
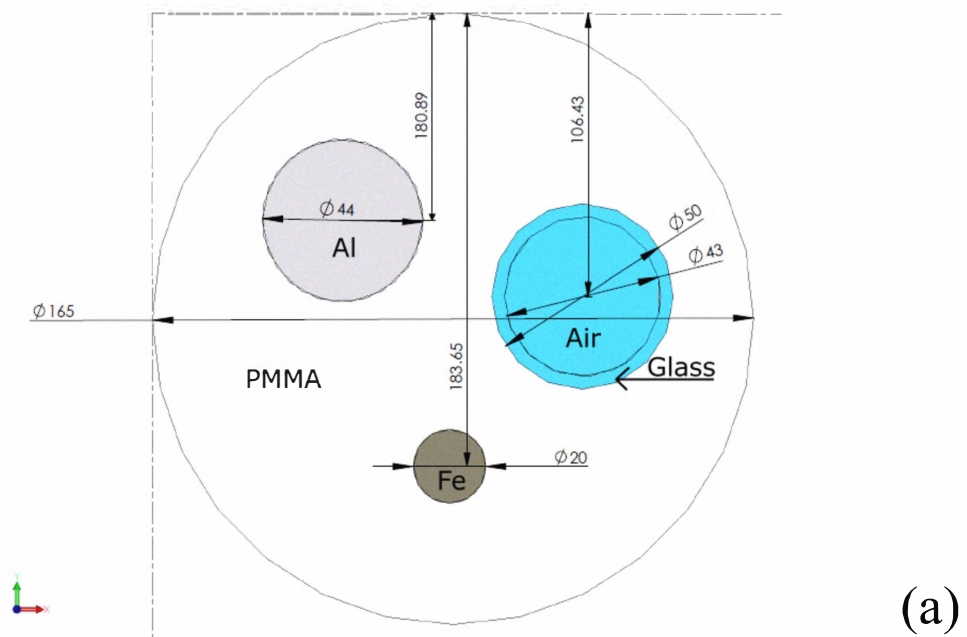


Fig. 10 – Phantom used to characterize the 3<sup>th</sup>-generation CT, operated with multichannel data acquisition. (a) Geometrical dimensions, (b) physical aspects and (c) theoretical image used to calculate the  $\text{RMSE}(\mu)$  in the equations (10).

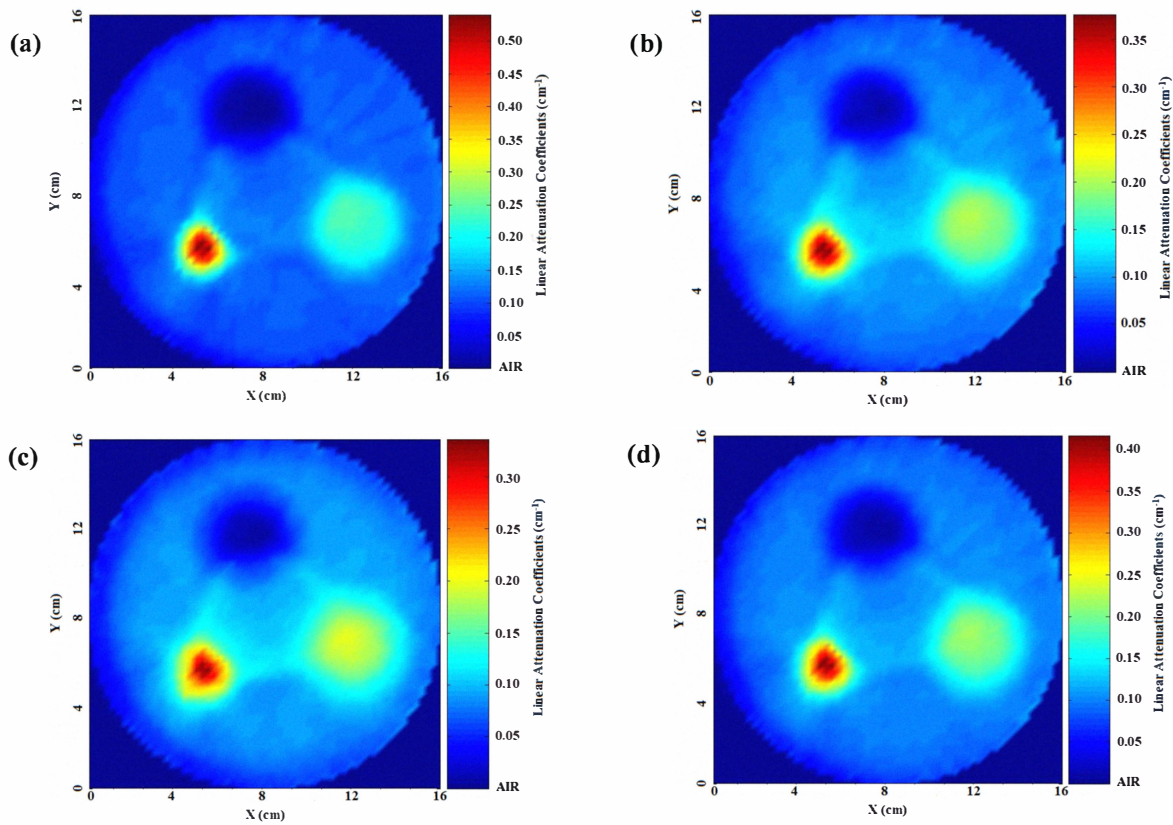


Fig. 11. Attenuation coefficient distributions for;  $^{192}\text{Ir}$  (317 keV) (a);  $^{192}\text{Ir}$  (468 keV) (b),  $^{137}\text{Cs}$  (662 keV) (c) and Open window  $\sim$ (50 keV to 800 keV) (d).

Table 1. Root Mean Squared Error for  $\mu$  (attenuation coefficient values) considering the whole object.

Isotope	Photopeak energy (keV)	RMSE( $\mu$ )
$^{192}\text{Ir}$	317	0.292
$^{192}\text{Ir}$	468	0.285
$^{137}\text{Cs}$	662	0.277

Table 2. Root Mean Squared Error for  $\mu$  (attenuation coefficient values), considering only the image regions containing different materials.

Material	RMSE( $\mu$ )		
	Energy (keV)		
	317	468	662
Air	<b>0.568</b>	0.589	0.586
Aluminum	<b>0.204</b>	<b>0.204</b>	0.216
Iron	0.844	<b>0.733</b>	<b>0.734</b>

#### IV - CONCLUSIONS

It was shown that the CT scanner is a viable tool to study multiphase systems. In fact, to study a three-phase ( $n=3$ )

system it is necessary to have two ( $n-1=2$ ) photopeak energies. This is the great advantage of this scanner, because it is capable to work with many sources placed in the same shielding system, since the electronic detection allows the accounting process in different channel regions, simultaneously. The use of fast multichannel counters, rather than single channels, allows the number of detectors and counters to be reduced, what simplifies substantially the third generation CT scanner, with the advantage of spectral information. For a static phantom with three phases, the best results depends on the inserted materials in the object to be evaluated by the CT. The multichannel data acquisition system has fast speed for tomographic data acquisition.

#### ACKNOWLEDGMENTS

The authors would like to express their gratitude to the FAPESP (2011/17802-7); CNPq (620201/2008-8) and IAEA (Proc. BRA 08/31) for the financial support

#### REFERENCES

- [1] Calvo, W.A.P.; Hamada, M.M; Vasquez, P.A.S.; De Mesquita, C.H. Gamma-ray computed tomography Scanners for applications in multiphase system columns. Nukleonika, 2009; 54(2): 129-133.
- [2] Vasquez, S.P.A.; De Mesquita, C.H.; Hamada, M.M. Methodological analysis of gamma tomography system for

large random packed columns. *Applied Radiation and Isotopes*; 2010; 68: 658-661.

[3] BIEBERLE, M.; HAMPEL, U. Evaluation of a limited angle scanned electron beam x-ray CT approach for two-phase pipe flows. *Measurement Science and Technology*, v.17(8), p.2057-2065, 2006.

[4] LANGE, K.; CARSON, R. EM Reconstruction Algorithms for Emission and Transmission Tomography. *Journal of Computer Assisted Tomography*, v.8(2), p.306-316, 1984.

[5] O'SULLIVAN, J.A.; BENAC, J. Alternating Minimization Algorithms for Transmission Tomography. *Medical Imaging, IEEE Transactions*, v.26(3), p.283-297, 2007.

[6] BENAC, J. Alternating minimization algorithms for X-ray computed tomography : multigrid acceleration and dual energy application. 2005. Tese (Doutorado) - Washington University, St. Louis.

[7] CSISZÁR, I. Why Least Squares and Maximum Entropy? An Axiomatic Approach to Inference for Linear Inverse Problems. *Annals of Statistics* , v.9, p.2033-2066, 1991.

[8] SNYDER, D.L.; SCHULZ, T.J.; O'SULLIVAN, J.A. Deblurring Subject to Nonnegativity Constraints. *IEEE transactions on signal processing*, v.40(5), p.1143-1150, 1992.